Starch-menthol inclusion complex: structure and release kinetics

Linfan Shi – South China University of Technology

Helene Hopfer – Pennsylvania State University

Gregory R. Ziegler – Pennsylvania State University

Lingyan Kong – University of Alabama

Citation of published version:

Shi, L., Hopfer, H., Ziegler, G., Kong, L. (2019): Starch-menthol inclusion complex: structure and release kinetics. *Food Hydrocolloids*, vol. 97.

DOI: https://doi.org/10.1016/j.foodhyd.2019.105183

Full text at https://doi.org/10.1016/j.foodhyd.2019.105183
or send request to lingyan.kong@ua.edu

Starch-menthol inclusion complex: structure and release kinetics

Linfan Shi[ab], Helene Hopfer[a], Gregory R. Ziegler[a], Lingyan Kong[c,*]

[a] Department of Food Science, Pennsylvania State University, 341 Food Science Building, University Park, PA 16802, USA

[b] School of Food Science and Engineering, South China University of Technology, Guangzhou 510640, PR China

[c] Department of Human Nutrition and Hospitality Management, The University of Alabama, Tuscaloosa, AL 35487, USA

* Corresponding author at: 482 Russell Hall, Tuscaloosa, AL 35487, USA.

Tel.: +1 205-348-6940

E-mail addresses: lingyan.kong@ua.edu (L. Kong).

Abstract: Flavoring ingredients are often the most expensive ingredients in food formulations, and their stability and release behavior are significant factors for quality and acceptability of food products. Among flavoring compounds, aroma compounds draw a lot of attention in research, as their volatile nature makes their release difficult to control. In the present study, we employed pre-formed V-type starches to molecularly encapsulate an aroma compound, i.e., menthol. We examined high amylose maize starch of six different V-type crystalline structures (containing 6, 7 and 8 glucose units per helical turn), namely V_6, V_7, and V_8-types, to encapsulate menthol and thus, to control the release behavior. Rehydration of V_{6a} at a relative humidity of 0.75 lead to its conversion to V_{6h} (V_h), while rehydration had only minor influence on the XRD patterns of anhydrous forms of V_7 and V_8. Successful inclusion complexation was characterized by X-ray diffraction (XRD), differential scanning calorimetry (DSC), and gas chromatography-mass spectrometry (GC-MS). Upon complexation with menthol, the XRD pattern of V_{6h} shifted to V_7, whereas all other V-subtypes retained their original crystalline structures. An endotherm with peak temperature at ca. 118 °C appeared after inclusion complexation, corresponding to the dissociation of starch-menthol inclusion complexes. Endothermic enthalpy, with the exclusion of V_{6a}, and GC-MS quantification agreed that the total menthol content in inclusion complexes followed the order of $V_{6h} > V_{6a} > V_{7a} >$ "V_{7h}" $> V_{8a} >$ "V_{8h}," with the helices initially of the V_{6h}-type being the most effective in encapsulating menthol molecules. The controlled release characteristics of the encapsulated aroma compound were also investigated in the presence and absence of pancreatic α-amylase. The presence of amylase increased both the release rate and the amount of menthol

released within two hours. The release rates were different among samples made from different subtypes, due to their different association mechanisms with menthol, including physical adsorption on the surface of starch or in the amorphous phase, inter-helical entrapment, and intra-helical inclusion complexation. The Higuchi model was fitted to understand the release kinetics and showed that the constant *Y* for menthol release from different V-type ICs followed the order of "V_{8h}" > V_{8a} > "V_{7h}" > V_{6a} > V_{7a} > V_{6h}.

Keywords: Starch; Amylose; Encapsulation; Inclusion complex; Menthol; Release Kinetics.

1. Introduction

Flavor compounds, including volatile aroma compounds, are usually among the most valuable ingredients in any food formulation, and play an important role in consumer acceptance and satisfaction of food products (Madene, Jacquot, Scher, & Desobry, 2006). Most commercial aroma compounds are produced via chemical synthesis or extraction from natural sources, are of limited stability and medium to high volatility, making their preservation a top concern in the food industry. Encapsulating aroma compounds into solid matrices with controlled release properties may effectively improve their efficacy.

The encapsulation of flavor compounds, particularly volatile aroma compounds has been widely investigated in food science (Guichard, 2002; Madene, et al., 2006). Encapsulation of aroma compounds can improve their utility by reducing evaporation, preventing the loss of volatiles, and enhancing their stability during storage and application. Starch, especially its amylose component, forms inclusion complexes (ICs) with small molecules, including a number of aroma compounds, e.g., menthone (Tapanapunnitikul, Chaiseri, Peterson, & Thompson, 2007), menthol (Osman‐Ismail & Solms, 2010), thymol (Tapanapunnitikul, et al., 2007), geraniol (Nuessli, Putaux, Bail, & Buléon, 2003), and fenchone (Nuessli, et al., 2003). In these ICs, amylose forms a left-handed single helix with a hydrophilic outer surface and a hydrophobic inner helical cavity to accommodate the guest compounds. The ICs can pack together in a crystalline structure known as the V-type, which exists as a number of subtypes (Biais, Le Bail, Robert, Pontoire, & Buléon, 2006). The dimension of the V-amylose helix is controlled by the size of the complexed

guest, leading to helices with 6, 7, or 8 glucose residues per turn (Nuessli, et al., 2003). In the presence of small guest molecules, such as iodine (Bluhm & Zugenmaier, 1981) and fatty acids (Godet, Buléon, Tran, & Colonna, 1993; Le, Choisnard, Wouessidjewe, & Putaux, 2018), amylose forms 6-fold single helices (V_6). Helices of larger dimensions can be obtained when complexed guest molecules bulkier than linear alcohols are used. For instance, *tert*-butanol (Zaslow, 1963) and 2-propanol (Nishiyama, et al., 2010) complex with amylose to form 7-fold single helices (V_7). The guest compounds can also exist in the interhelical space as in the case of 2-propanol (Nishiyama, et al., 2010). The ICs formed by amylose and even larger/bulkier molecules, e.g., 1-naphthol and quinolone (Yamashita, Ryugo, & Monobe, 1973), contain 8-fold single helices (V_8) with larger cavities. The outer and inner diameters of the V_6-V_8 helices vary from 13.6 to 16.2 Å and from 5.4 to 8.5 Å, respectively (Cardoso, et al., 2007).

The V_{6a} has an orthorhombic unit cell structure with dimensions of approximately a = 13.0 Å, b = 23.0 Å, c = 8.05 Å (Rundle, 1947; Zobel, French, & Hinkle, 1967), while the V_{6h} form has a hexagonal unit cell with parameters a = b = 13.65 Å, c = 8.05 Å (Brisson, Chanzy, & Winter, 1991). The only difference between V_{6a} and V_{6h} is the number of water molecules in the unit cells, which induces slight modifications to their crystal structure (Obiro, Sinha Ray, & Emmambux, 2012). Practically, V_{6a} can be transformed to V_{6h} by exposure to a humid environment (e.g., 85% relative humidity), while V_{6h} can be dehydrated by drying to form V_{6a}.

Starch/amylose ICs may be useful as a delivery system for guest molecules, such as conjugated linoleic acid (Lalush, Bar, Zakaria, Eichler, & Shimoni, 2005), genistein (Cohen,

Schwartz, Peri, & Shimoni, 2011), and poly-unsaturated fatty acids (Lesmes, Cohen, Shener, & Shimoni, 2009). In addition to the protective effect of starch ICs, the release of guest compounds can be regulated by the action of digestive enzymes, such as salivary and pancreatic α-amylase. In the case of aroma compounds, triggered and prolonged release may be achieved by using starch ICs.

Here we investigated the capability of various V-subtypes of high amylose maize starch (HAMS) to encapsulate menthol and the release properties of menthol from its HAMS ICs upon enzymatic digestion. Menthol was complexed by direct contact with the preformed "empty" V-type HAMS allomorphs at a temperature above its melting point. The formation of ICs was characterized by X-ray diffraction (XRD) and differential scanning calorimetry (DSC). Gas chromatography-mass spectrometry (GC-MS) was used to quantify total menthol content in the ICs and headspace GC-MS (HS-GC-MS) was used to monitor menthol release. This study allowed us to determine the best complexation method for menthol and determine its release profile from the ICs, in particular for its enzymatically controlled release**.**

2. Materials and methods

2.1. Materials

High amylose maize starch (HAMS; Gelose 80) was kindly provided by Ingredion (Bridgewater, NJ, USA). L-Menthol (99%) was purchased from Sigma-Aldrich, Inc. (St. Louis, MO, USA). Acetone (HPLC grade) was obtained from EMD Millipore Chemicals (Billerica, MA, USA). Ethanol (200 proof) and dimethyl sulfoxide (DMSO) were obtained from VWR

International (Radnor, PA, USA). Pancreatic α-amylase was purchased from Megazyme (Chicago, IL, USA). Salicylic acid and *tert*-butanol were obtained from Thermo Fisher Scientific (Waltham, MA, USA). All reagents, if not otherwise specified, were of analytical grade.

2.2. Preparation of V-subtypes of HAMS

The V_{6a}-type HAMS with "empty" helical cavities was prepared according to an established procedure (Kong & Ziegler, 2014b). HAMS (5%, w/v) was dissolved in 95% (v/v) aqueous DMSO solution in a boiling water bath with constant stirring for at least 1 hour. The hot dispersion was mixed into 2.5 volumes of pure ethanol at 20 °C with vigorous stirring, the mixture centrifuged (2000 g, 10 min), and the supernatant discarded. The precipitate was washed twice with pure ethanol and finally dried in a vacuum desiccator. The dry powders were then annealed in 40% (v/v) aqueous ethanol solution in a 70 °C water bath for 1h, washed with pure ethanol, and re-dried to obtain the V_{6a}. The V_{6h} sample was obtained by conditioning the V_{6a} sample in a desiccator containing saturated NaCl solution (a_w=0.75) for 1 day.

The V_{7a}-type HAMS was obtained by heating the V_{6h} sample with *tert*-butanol (amylose:*tert*-butanol = 1:4, w/w) at 90 °C in a sealed pressure vessel for 30 min, followed by vacuum drying in order to evaporate *tert*-butanol. The V_{7a}-HAMS was then conditioned in a desiccator containing saturated NaCl solution (a_w=0.75) for 1 day to obtain the rehydrated "V_{7h}-type". The V_{8a}-type HAMS was produced by heating the V_{6h}-HAMS with salicylic acid (amylose:salicylic acid = 1:1, w/w) in a sealed pressure vessel at 150 °C for 1 hour. The product was then washed with excess acetone to remove all salicylic acid and vacuum dried. The rehydrated "V_{8h}-type" was then

obtained by conditioning the V_{8a} type in a desiccator containing saturated NaCl solution (a_w=0.75) for 1 day. All V-type samples were further degassed at 50 °C (V_h samples) or 110 °C (V_a samples) for 16 h using a Micromeritics VacPrep 061 degasser (Micromeritics Instrument Corporation, Norcross, GA, USA) attached to a heating station.

2.3. Inclusion complexation with menthol

The V-type HAMS samples were heated with an equal weight of menthol in a sealed pressure vessel at 70 °C for 30 min. The mixture was then washed with 10 mL of pure ethanol twice at 20 °C and collected by the same drying procedure as described above to remove uncomplexed menthol.

2.4. Quantification of total menthol content in ICs

The total menthol content (w/w) in the ICs was determined by dissociation of ICs using an alkali solution, extraction of menthol using ethyl acetate, and quantification using gas chromatography-mass spectrometry (GC-MS). In detail, 5 mg of IC sample was mixed into 0.5 mL of 0.1 M KOH solution in a 2 mL microcentrifuge tube. The dispersion was vigorously mixed using a vortex mixer to dissolve the IC powders, and a clear solution was obtained. Then, 0.5 mL of ethyl acetate was added with vigorous mixing using a vortex mixer for 30 s. The mixture was centrifuged (9,391 × *g*, 1 min) for complete separation. The supernatant was collected and its menthol content was quantified by gas chromatography-mass spectrometry (GC-MS).

2.5. Gas chromatography-mass spectrometry (GC-MS)

A GC-MS system (7890B and 5977B, Agilent, CA, USA) with an automatic autosampler (Gerstel Robotic, Linthicum, MD, USA) was used for all GC-MS measurements. The sample or standard (1 µL) was injected into the GC in split mode (20:1), using an inlet temperature of 220 °C and an oven program as follows: start temperature 80 °C with a hold of 1 min, ramped 30 °C/min to 250 °C, with a final hold of 2 min. A Stabilwax-MS capillary column (30 m × 0.25 mm × 0.25 µm, Restek, Bellefonte, PA, USA) was used with a carrier gas flow of ultrapure helium (99.999%; Praxair, State College, PA, USA) at a rate of 1.15 mL/min. The MS transfer line, quadrupole, and detector temperatures were set to 250 °C, 230 °C, and 150 °C, respectively. Compounds were detected in simultaneous scan (33-350 m/z with 14 scans/sec) and selected ion monitoring (SIM) mode (95, 123; dwell time of 75 ms). Peaks were integrated in MSD ChemStation software (version F.01.03.2357, Agilent Technologies, CA, USA), and identified with the NIST 14 spectral library (version 2.2.) and authentic standards ranging from 0.01-0.25 g/L (R^2=0.99). For the release kinetics measurements, the same instrument and conditions were used, except for the inlet temperature (250 °C) and the oven program (start temperature of 100 °C ramped with 50 °C/min to 250 °C; total run time 3 min).

2.6. Wide angle X-ray diffraction (XRD)

XRD patterns were obtained using a Rigaku MiniFlex II desktop X-ray diffractometer (Rigaku Americas Corporation, TX, USA). Dried sample powders were exposed to Cu Kα radiation

(λ=0.154 nm) and continuously scanned from 4 to 30° 2θ at a scan rate of 0.5°/min with a 0.02° step interval.

2.7. Differential scanning calorimeter (DSC)

Approximately 5-6 mg of dry sample was weighed using a Mettler-Toledo XP2U ultra-microbalance (Mettler-Toledo International Inc., Columbus, OH, USA) into a large-volume stainless steel DSC pan (Perkin-Elmer Instruments, Norwalk, CT, USA). Deionized water was added to obtain a 10% (w/v) dispersion. The DSC Pan was hermetically sealed. Using an empty pan as the reference, the pans were equilibrated to 10 °C, and then heated to 150 °C at 10 °C/min in a Thermal Advantage Q100 DSC (TA Instruments, New Castle, DE, USA). Data was analyzed using the TA Universal Analysis software (Universal Analysis 2000 v.4.2E, TA Instruments-Waters LLC, New Castle, DE, USA).

2.8. Release kinetics of menthol

To evaluate the release of menthol from ICs upon hydrolysis with and without α-amylase, headspace (HS) menthol content above the reaction medium was measured by HS-GC-MS. Pancreatic α-amylase (50 mg) was suspended in sodium acetate buffer (100 mM, pH = 5.0, 10 mL) and stirred for 5 min prior to use. IC samples (5 mg) were added into α-amylase solution (1 mL) in a 20 mL headspace vial, and the vial was immediately capped with a magnetic cap (Restek Corporation, Bellefonte, PA, USA). Samples were thermostated at 37 °C in the autosampler during analysis. Headspace samples (1 mL) were taken at 0, 1, 5, 9, 13, 17…120 min using a 2.5 mL HS syringe, and every HS extraction lasted 30 s. For the 0 min time point, the 1 mL HS sample was

taken at 10 s after the addition of α-amylase solution to the IC sample. As a control, ICs were mixed with 1 mL of sodium acetate buffer without pancreatic α-amylase.

To study the release kinetics, the data obtained from menthol release studies were fitted with the Higuchi model (Higuchi, 1961), which is based on Fickian diffusion, and follows a linear relationship between the drug released from the matrix and the square root of time. The Higuchi model is described as Eq. (1):

$$Q_t = k_H \times t^{1/2} \quad (1)$$

where Q_t is the amount of menthol released at the time t, k is the rate constant for the Higuchi rate equation, and t is the time in minutes. When a plot of cumulative drug release vs. $t^{1/2}$ yields a straight line, the system follows Higuchi kinetics.

2.9. Statistical analysis

The results are recorded as the means ± standard deviation, and significant differences between groups were tested using one-way analysis of variance (ANOVA) and Fisher's Least Significant Difference (LSD) test at $p < 0.05$. Statistical analysis was conducted using SPSS version 19.0 software (SPSS, Inc., Chicago, IL, USA).

3. Results and discussion

3.1 Characterization of HAMS V-subtypes

XRD patterns (Fig. 1A) were obtained to confirm the formation of various preformed "empty" V-subtypes of HAMS. The V_{6a}- and V_{6h}-types showed major diffraction peaks at 2θ = 7.9°, 13.7°, and 21.0° (corresponding d-spacing of 1.118 nm, 0.646 nm, and 0.423 nm), and at 2θ = 7.6°, 13.0°

and 20.1° (corresponding d-spacing of 1.162 nm, 0.680 nm, and 0.441 nm), respectively. These values were very close to those reported previously (Kong, et al., 2014b; Zobel, et al., 1967). The V_{7a}- and "V_{7h}-type" showed major diffraction peaks at 2θ = 7.2°, 12.2°, and 18.6° (corresponding d-spacing of 1.226 nm, 0.725 nm, and 0.675 nm), and at 2θ = 7.0°, 12.1°, 18.3° (corresponding d-spacing of 1.244 nm, 0.731 nm, and 0.670 nm), respectively. The V_{8a}-type was characterized by three major peaks at 2θ = 6.4°, 12.9°, and 16.8° (corresponding d-spacing of 1.379 nm, 0.685 nm, and 0.527 nm), whereas the "V_{8h}-type" showed diffraction peaks at 2θ = 6.2°, 12.7°, and 16.6° (corresponding d -spacing of 1.424 nm, 0.696 nm, and 0.533 nm). The major diffraction peaks of V_7-types agreed with those reported by Nuessli, et al. (2003) for amylose-fenchone inclusion complex after drying. The diffraction patterns of both V_7 and V_8 types were also close to those reported for amylose inclusion complexes with salicylic acid and its analogues (Oguchi, Yamasato, Limmatvapirat, Yonemochi, & Yamamoto, 1998; Uchino, Tozuka, Oguchi, & Yamamoto, 2002). The diffraction peak at 2θ = 21° shifted roughly 1° to lower angles when the V_{6a} was hydrated to V_{6h}, suggest that water molecules penetrated the interhelical space of the V_{6a}-type, increasing the interhelical distance, while the V_{7a}- and V_{8a}-types experienced only a 0.2-0.3° peak shift when they were rehydrated. In the case of the V_{7a}- and V_{8a}-types, the spacing between adjacent helices was only slightly, if at all, enlarged by the addition of water molecules. The intra- and interhelical spaces may already have enough room for the water molecules without the need for expansion, or water molecules found it difficult to enter the crystalline phase of the V_{7a}- and V_{8a}-types. Nuessli et al. (2003) demonstrated that drying of amylose-fenchone ICs reduced the rather complex XRD

patterns to ones with only three broad reflections that remained even after rehydration at a relative humidity of 0.75, and concluded that the diagrams did not correspond to the hexagonal Vh type, but did comprise sevenfold helices. Here we designate V_{7h} and V_{8h} as those samples comprising 7- and 8-fold helices, respectively, rehydrated at a relative humidity of 0.75 without assuming they are hexagonal "Vh" forms (hence "V_{7h}" and "V_{8h}").

Thermograms of the "empty" V-subtypes showed no noticeable endotherms in comparison with their ICs (Fig. 2A & B). Although a small amount of lipids, such as palmitic, stearic, and linoleic acid, are present in native HAMS, the preparation procedures may have removed these endogenous lipids. Hence, no endotherm around 60-90 °C in the V_6-types was observed as was the case in some of our previous reports (Kong & Ziegler, 2014a). An endotherm in this range may also be attributed to the retrogradation of the amylopectin fraction of starch (Kohyama & Nishinari, 1991). The minor response between 80-90 °C in thermograms of the V_8-types was possibly due to HAMS-salicylic acid inclusion complex that survived the washing and extraction process. None of the V-subtypes showed any notable endotherm above 120 °C that could be attributed to retrograded or recrystallized amylose molecules. Combined XRD and DSC evidence suggested that all V-subtypes prepared comprised essentially "empty" helices that could be available to accommodate guest molecules, e.g., menthol.

3.2. HAMS-menthol inclusion complexes

ICs were prepared by directly reacting menthol with various V-types of HAMS at an elevated temperature (70 °C). XRD patterns of the HAMS-menthol ICs are shown in Fig. 1B. Compared

245 with those of the “empty” samples (Fig. 1A), the diffraction peaks of ICs became less sharp,
246 indicating a decrease in crystallinity. The decrease in crystallinity could be due to either the loss
247 of water molecules that plasticize and stabilize helical packing, or the entrapment of menthol
248 molecules between helices or within crystalline regions, leading to distorted and less regular
249 packing. No major peak shift was observed upon inclusion complexation with menthol in all but
250 the V_{6h}-type. The 7.6° and 20.1° peaks of the V_{6h}-type HAMS shifted to 6.7° and 18.3°,
251 respectively, which are typical of V_7 diffraction (Ades, Kesselman, Ungar, & Shimoni, 2012).
252 Inclusion of menthol molecules into the V_{6h}-type expanded the helical cavity to the size of a V_7
253 helix (from here on the reader should read V_{6h}-IC as that complex formed from what originally
254 was V_{6h} despite having V_7 character after inclusion of menthol). The V_{6a}-type helix, on the other
255 hand, was not expanded by menthol molecules, indicating that menthol was not entrapped within
256 its helical cavity. The difference in the response of V_{6a} and V_{6h} structures could be explained by
257 different molecular mobility in the anhydrous and hydrated states of the HAMS helices; the V_{6h}
258 helices are more mobile and flexible due to the presence of water molecules. The V_7- and V_8-types
259 did not experience peak shifts, because their helical cavities did not need to be expanded to entrap
260 menthol molecules. It was noticed that menthol complexation with V_{6h}-, and V_7-types gave
261 diffraction patterns that were a superposition of V_7 and V_{6a} polymorphs, indicated by a small peak
262 at around 2θ = 21°. We suggest that menthol encapsulation did not reach its maximum loading
263 capacity, which is an important parameter in aroma encapsulation. The helices of any V-subtype,
264 if left empty, could be converted to V_{6a}-type by ethanol during the washing procedure. The ethanol

washing procedure could also extract and remove some complexed menthol molecules from the ICs and convert the empty helices to V_{6a}-type. There was no difference in XRD peak angles between the two empty V_8-types and their ICs, although the diffraction peaks of ICs appeared less sharp. Either more menthol molecules could be stacked inside the V_8 helices, as in the proposed mechanism of salicylic acid (Oguchi, et al., 1998), or menthol molecules did not interact sufficiently with the large V_8 helical cavity. Quantification of menthol content in V_8-types seemed to indicate the latter, which will be described below.

The dissociation temperatures of the ICs were evaluated by DSC (Fig. 2B and Table 2). Variations in onset temperature (T_0), peak temperature (T_p), conclusion temperature (T_c), and enthalpy (ΔH) of endotherms have been shown to reflect the crystallinity, structure, and composition of starches, including the V-types (Lay Ma, Floros, & Ziegler, 2011). In the DSC thermograms of ICs, the T_p indicates the thermal stability of the ICs, which is affected by the identity of guest and lamellar thickness, while ΔH reflects the amount of guest molecules included. In contrast to the empty V-types, all ICs displayed an endotherm with T_p at around 118 °C, except for a small peak at 88 °C in V_{7a}. The V_{6a}-IC had a small endotherm with ΔH of only 0.49 ± 0.12 J/g, indicating only minimal menthol inclusion. The complex originally V_{6h} had the largest endothermic peak with ΔH of 13.68 ± 0.20 J/g, followed by V_{7a}, "V_{7h}", V_{8a} and "V_{8h}" in a descending order, consistent with their total menthol contents (described below). Within V_7- and V_8-types, the rehydrated forms showed smaller endotherms, suggesting that the presence of water

molecules might interfere with menthol complexation, despite making the helices more flexible, perhaps by altering the hydrophobicity of the helix interior thereby influencing partitioning.

The menthol content in ICs was quantified by GC-MS, following its liberation by alkali dissolution and liquid-liquid extraction. The menthol content in ICs differed significantly ($p < 0.05$) and followed the order of $V_{6h} > V_{6a} > V_{7a} >$ "V_{7h}" $> V_{8a} >$ "V_{8h}" (Fig. 3). The quantified menthol content and the ΔH of the ICs showed a linear relationship ($Total\ menthol = 0.38 \times \Delta H - 0.49$; R^2=0.95), if not considering the V_{6a}-IC. It means that the measured total menthol was mainly, or at least proportional to, the menthol encapsulated in the ICs. More than expected menthol was extracted from V_{6a}-IC and the extra menthol could have been entrapped between the helices or within the amorphous regions. Some researchers suggested that guest molecules could be located between helices (Nishiyama, et al., 2010; Rondeau-Mouro, Le Bail, & Buléon, 2004), while it is also reasonable to expect them to be physically entrapped within the amorphous regions (Conde-Petit, Escher, & Nuessli, 2006). However, why menthol should be preferentially adsorbed to V_{6a} over the other V-subtypes is unknown, perhaps our ethanol washing was less effective in this sample. The loading capacity of menthol in ICs was apparently dependent on the size of helical cavity and the hydration state of the crystalline V-types. The helices initially of the V_{6h}-type seemed to be the most effective structure to molecularly encapsulate menthol.

3.3. Release kinetics of menthol

The enzymatic digestion of starch ICs has been widely studied, and is a determinant factor for its nutritional value and use as a delivery system (Tan & Kong, 2019). An interesting aspect of

304 starch-aroma ICs is that the release of aroma compounds can be influenced by enzymes, such as
305 α-amylase, marking its potential use for triggered or sustained release of aroma in food
306 formulations. Ades, et al. (2012) incubated the HAMS-menthol ICs in simulated saliva fluids
307 (37 °C, pH 7.2, 100 u/ml, 12 rpm), and full menthol release was achieved after 4 h of hydrolysis
308 by α-amylase. To assess the release behavior of encapsulated menthol from ICs in the present
309 study, headspace menthol concentration was monitored over 2 h above buffer with or without
310 pancreatic α-amylase (Fig. 4). The rate of menthol release from all ICs was the fastest in the first
311 10 min, slowing thereafter. In the case of V_6- and V_7-type ICs, the presence of α-amylase
312 significantly increased the amount of menthol released, compared to their control groups without
313 the enzyme. The extent of menthol release was identical in V_8-type ICs with and without the
314 addition of α-amylase. The amount of menthol released from ICs upon enzymatic hydrolysis
315 followed the order of $V_{6h} > V_{6a} > V_{7a} >$ "V_{7h}" $> V_{8a} >$ "V_{8h}", which was consistent with the trend
316 of total menthol content in the ICs quantified by GC-MS (Fig. 3).

317 There can be two mechanisms of menthol release, corresponding to two mechanisms of
318 encapsulating menthol in ICs, including both specific, i.e., inclusion complexation, and non-
319 specific binding, i.e., physical sorption and/or entrapment (Conde-Petit, et al., 2006). Regardless
320 of enzyme addition, there was a spike of menthol release during the first 10 min. This portion of
321 menthol seemed to be loosely or weakly associated with the HAMS by two possible non-specific
322 binding mechanisms, i.e., physical sorption on particle surfaces and physical entrapment in
323 amorphous regions. Extensive washing during the IC making procedure should have removed

menthol adsorbed on surface and pores, therefore, the menthol released at the beginning would be from the amorphous regions. The amorphous regions contain loosely and irregularly associated starch molecules and menthol molecules that are more susceptible to moisture penetration than the crystalline regions. As the amorphous regions were hydrated, menthol would partition between the buffer and the headspace for detection. In the presence of α-amylase, the enzyme could digest the amorphous starch molecules and accelerate the release of menthol.

The greater extent of menthol release from the V_6- and V_7-types of ICs in the presence of α-amylase is further evidence of the encapsulation of menthol in the IC helices. ICs are not soluble in water or the buffer, and thus complexed menthol would not be released without addition of enzyme. The ICs can be digested by α-amylase, albeit perhaps incompletely within 2 h of digestion in this study. A portion of "resistant" ICs could remain, although it was not determined in this study. There was no significant difference in menthol release pattern between V_8-ICs in the presence and absence of pancreatic α-amylase. The larger diameter of the V_8 helices would require the hydrophobic interactions that stabilize the complex to exert their influence over a longer distance. Perhaps these forces were insufficient to retain the menthol once the complex was dispersed in the buffer. The extent of menthol release from V_6-, V_7-, and V_8-type ICs agrees with the trend of encapsulated menthol content from DSC and total menthol content data. These results showed that V_{6h}-type HAMS has the highest menthol loading using the experimental method in this study.

The release data in the first 10 min were analyzed by the Higuchi model (Higuchi, 1961). The Higuchi model was originally used to describe the quantification of drug release from thin ointment films, containing finely dispersed drug into a perfect sink. Based on a pseudo-steady-state approach, a direct proportionality between the cumulative amount of drug released and the square root of time could be demonstrated. The equation can also be applied to other types of drug delivery systems other than thin ointment films, e.g., controlled release transdermal patches or films for oral controlled drug delivery (Siepmann & Peppas, 2011). In the present study of menthol release from ICs, the rate constant (k_H) and unit rate constant (Y) are summarized in Table 3. Since k_H is the rate constant determined by both the matrix internal structure and the initial menthol concentration, it was normalized by menthol content to compare the unit menthol release (Eq. 2).

$$Y = k_H / total\ menthol\ content \quad (2)$$

Y represents the release rate constant of the unit menthol content, which could describe release rate of the menthol from the ICs. The Y followed the order of "V_{8h}" > V_{8a} > "V_{7h}" > V_{6a} > V_{7a} > V_{6h}, which indicated that the menthol has the strongest binding strength with V_{6h}, and the weakest binding strength with "V_{8h}". A similar trend was found for the ICs in the absence of α-amylase in the sodium acetate buffer. In the case of V_{6a}-IC, most menthol was physically entrapped in the amorphous regions, whereas V_{6h}-type could encapsulate most menthol molecules in the helices. The amorphous regions in V_{6a} are susceptible to water, and thus V_{6a}-IC released menthol faster than V_{6h}-IC and even V_{7a}-IC. For V_7- and V_8-types, the hydrated forms showed higher release rates, possibly due to higher mobility of molecules in the hydrated forms. There were significant

differences in the *Y* values of V_6- and V_7-ICs in the present and absence of α-amylase, whereas the presence of the enzyme did not affect the *Y* values of V_{8a}-IC and "V_{8h}"-IC, in agreement with our findings above that menthol was encapsulated into the helices in V_6- and V_7-ICs, while V_8-type helices might not be suitable for entrapping menthol molecules.

4. Conclusions

In the present study, we successfully demonstrated the capability of a series of pre-formed V-type HAMS to molecularly encapsulate menthol, an aroma compound, in ICs. The total menthol content in ICs followed the order of V_{6h} > V_{6a} > V_{7a} > "V_{7h}" > V_{8a} > "V_{8h}", and the V_{6h}-type was the most effective in encapsulating menthol molecules. The XRD pattern of V_{6h} shifted to V_7 upon menthol complexation, whereas all other V-types retained their original crystalline structure. This indicates that menthol expanded the helical cavity of the V_{6h} to the size of the V_7-type for it to be encapsulated. The HAMS-menthol ICs showed an endotherm with peak temperature around 118 °C. Release studies suggested the coexistence of different binding mechanisms of menthol in the HAMS IC matrix that include non-specific physical entrapment in amorphous regions and specific binding in IC single helices. The presence of α-amylase significantly increased the release rate and the released amount of menthol from V_6 and V_7-type ICs within 2 h. It indicated that the addition of amylase accelerated the release of menthol from amorphous regions and triggered its release from ICs. A Higuchi model was used to analyze the menthol release kinetics. The normalized rate constant *Y* for menthol release from different V-type ICs followed the order of "V_{8h}" > V_{8a} > "V_{7h}" > V_{6a} > V_{7a} > V_{6h}, suggesting V_{6h} was the most effective type to form inclusion

complex with menthol, whereas the V_8 type was not capable of forming complexes. This study demonstrated the pre-formed V-type starch as a promising delivery system for flavor compounds, the release of which can be triggered and controlled by the action of digestive enzyme, such as pancreatic α-amylase.

Abbreviations

DSC, differential scanning calorimetry; HS-GC-MS, headspace-gas chromatography-mass spectrometry; ICs, inclusion complexes; XRD, X-ray diffractometry.

Acknowledgments

This project is funded by the USDA National Institute for Food and Agriculture, Agriculture and Food Research Initiative Program, Competitive Grants Program award from the Improving Food Quality (A1361) program FY 2018 as grant # 2018-67017-27558. The China Scholarship Council is acknowledged for sponsoring L. Shi as a visiting student at the Pennsylvania State University. This work was also supported by the USDA National Institute of Food and Agriculture Federal Appropriations under project PEN04624 and accession number 1013412 to H. Hopfer, and under project PEN04565 and accession number 1002916 to G.R. Ziegler.

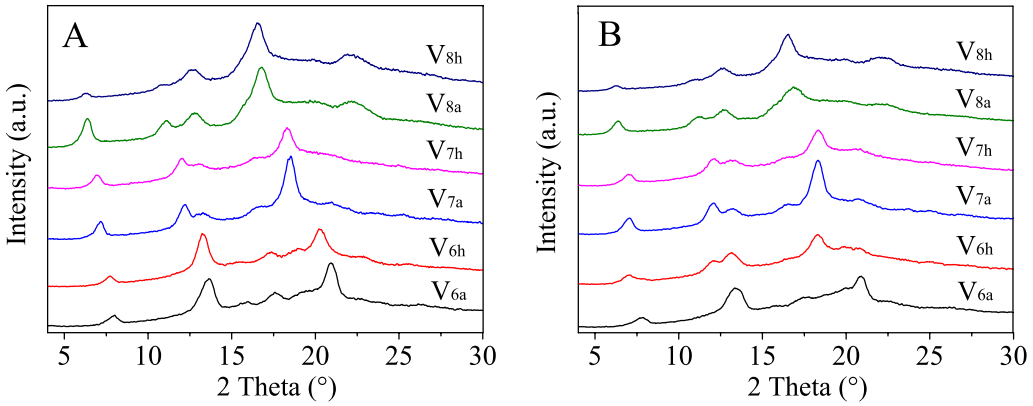

Fig. 1. X-ray diffraction patterns of V-type starches (A) and their inclusion complexes with menthol (B). Patterns are labeled with the polymorphic type of the starting V-type starch material.

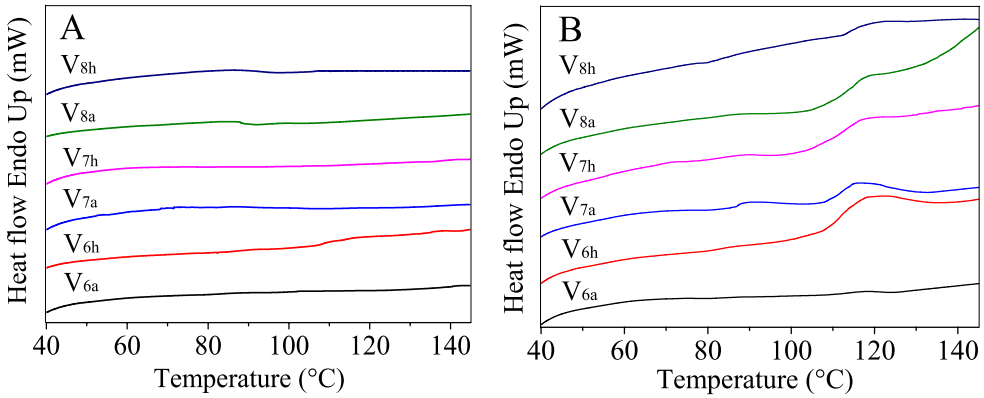

403

404 Fig. 2. DSC thermograms of V-type starches (A) and their inclusion complexes with

405 menthol (B). Patterns are labeled with the polymorphic type of the starting V-type starch

406 material.

407

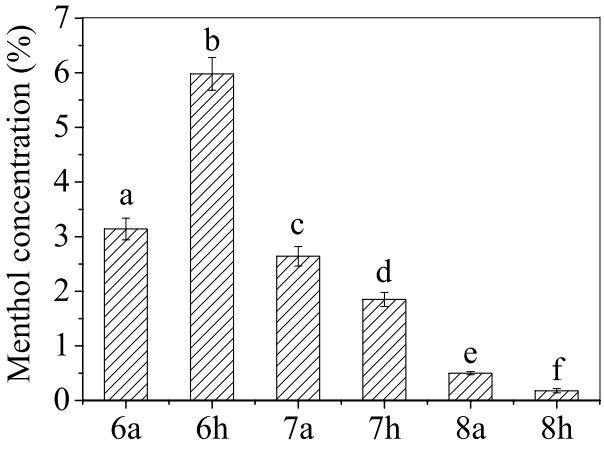

408

409 Fig. 3. Total menthol content (%, w/w) in V-type starch inclusion complexes.

410 Samples with different letters above the columns are significantly different at $p < 0.05$.

411 Patterns are labeled with the polymorphic type of the starting V-type starch material.

412

413

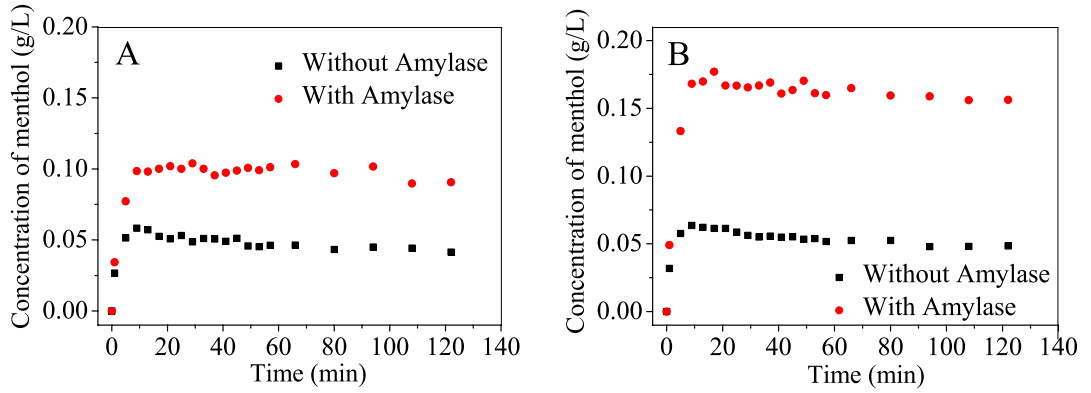

414

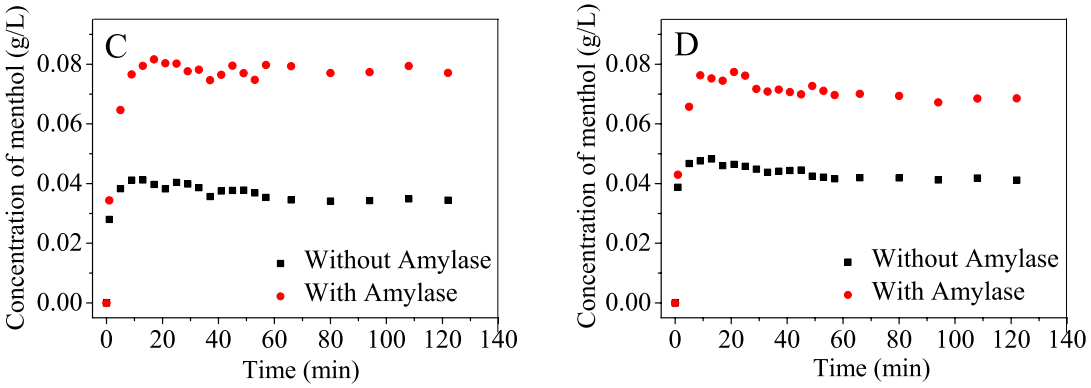

415

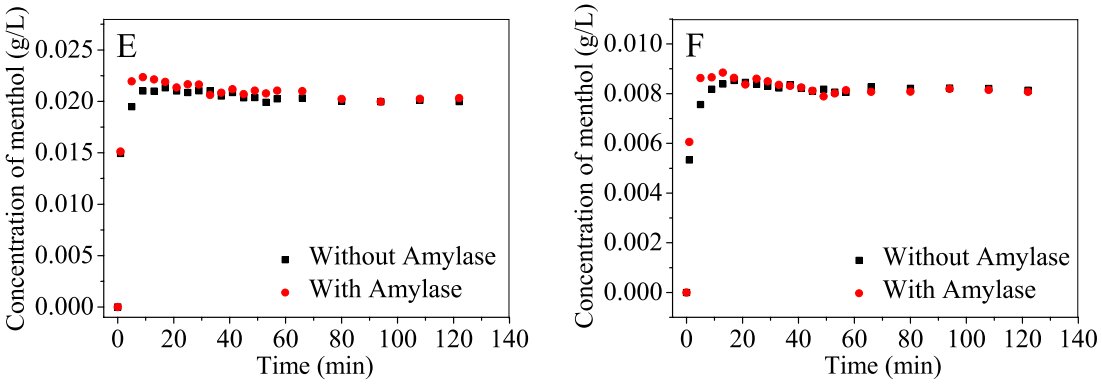

416 Fig. 4. Release profiles of menthol from inclusion complexes formed with V_{6a} (A), V_{6h}

417 (B), V_{7a} (C), "V_{7h}" (D), V_{8a} (E), and "V_{8h}" (F) starches, in the presence and absence of α-

418 amylase in the sodium acetate buffer (pH=5.0).

419

Table 1. Summary of main XRD peaks and corresponding d-spacings of various pre-formed V-type starches and their inclusion complexes menthol (IC).

Samples	2θ (°)		d-spacing (nm)	
	V-type starch	IC	V-type starch	IC
	7.9	7.9	1.118	1.118
V_{6a}	13.7	13.4	0.646	0.660
	21.0	20.9	0.423	0.425
	7.6	7.1	1.162	1.244
V_{6h}	13.0	13.0	0.680	0.680
	20.1	18.3	0.441	0.484
	7.2	7.2	1.226	1.226
V_{7a}	13.1	13.2	0.725	0.670
	18.6	18.3	0.675	0.484
	7.1	7.0	1.244	1.261
"V_{7h}"	13.2	13.3	0.731	0.665
	18.3	18.3	0.670	0.484
	6.4	6.4	1.379	1.379
V_{8a}	12.9	12.9	0.685	0.685
	16.8	16.8	0.527	0.527
	6.2	6.1	1.424	1.447
"V_{8h}"	12.7	12.7	0.696	0.696
	16.6	16.5	0.533	0.537

Table 2. Thermal properties of starch-menthol inclusion complexes (IC)[a]. Reported are averages ± standard deviation (n=2) of onset temperature T_o, peak temperature T_p, conclusion temperature T_c, and enthalpy change ΔH.

Samples	T_o (°C)	T_p (°C)	T_c (°C)	ΔH (J/g)
V_{6a}	110.39 ± 0.2[a]	117.88 ± 0.45[a]	123.75 ± 0.19[a]	0.49 ± 0.12[a]
V_{6h}	108.59 ± 0.37[b]	118.06 ± 0.22[a]	142.02 ± 0.37[b]	13.68 ± 0.20[b]
V_{7a}	109.79 ± 0.29[c]	118.14 ± 0.31[a]	131.25 ± 0.23[c]	9.31 ± 0.18[c]
"V_{7h}"	109.00 ± 0.38[b]	117.83 ± 0.38[a]	132.50 ± 0.30[d]	6.14 ± 0.23[d]
V_{8a}	111.46 ± 0.23[d]	118.27 ± 0.28[a]	130.27 ± 0.27[e]	2.84 ± 0.26[e]
"V_{8h}"	112.78 ± 0.2[e]	118.45 ± 0.31[a]	132.28 ± 0.29[d]	1.60 ± 0.19[f]

[a] Means in a column with different superscript letters are significantly different ($p < 0.05$) by Fisher's Least Significant Difference (LSD) test.

Table 3. Release rate constant (k_H) and unit rate constant (Y) of menthol released from inclusion complexes with V_{6a}, V_{6h}, V_{7a}, "V_{7h}", V_{8a}, and "V_{8h}" starches, based on Higuchi model in the presence and absence of α-amylase in sodium acetate buffer (pH=5.0).

Samples	With Amylase		Without Amylase	
	k_H	Y^a	k_H	Y^a
V_{6a}	0.0332	0.0106	0.0197	0.0063
V_{6h}	0.0578	0.0096	0.0214	0.0036
V_{7a}	0.0260	0.0098	0.0157	0.0059
"V_{7h}"	0.0256	0.0137	0.0132	0.0071
V_{8a}	0.0071	0.0139	0.0067	0.0128
"V_{8h}"	0.0028	0.0156	0.0026	0.0144

[a] $Y=k_H$/total menthol content

Reference:

Ades, H., Kesselman, E., Ungar, Y., & Shimoni, E. (2012). Complexation with starch for encapsulation and controlled release of menthone and menthol. *LWT - Food Science and Technology, 45*(2), 277-288.

Biais, B., Le Bail, P., Robert, P., Pontoire, B., & Buléon, A. (2006). Structural and stoichiometric studies of complexes between aroma compounds and amylose. Polymorphic transitions and quantification in amorphous and crystalline areas. *Carbohydrate Polymers, 66*(3), 306-315.

Bluhm, T. L., & Zugenmaier, P. (1981). Detailed structure of the Vh-amylose-iodine complex: a linear polyiodine chain. *Carbohydrate Research, 89*, 1-10.

Brisson, J., Chanzy, H., & Winter, W. T. (1991). The crystal and molecular structure of VH amylose by electron diffraction analysis. *International Journal of Biological Macromolecules, 13*, 31-39.

Cardoso, M. B., Putaux, J.-L., Nishiyama, Y., Helbert, W., Hÿtch, M., Silveira, N. P., & Chanzy, H. (2007). Single crystals of V-amylose complexed with α-naphthol. *Biomacromolecules, 8*, 1319-1326.

Cohen, R., Schwartz, B., Peri, I., & Shimoni, E. (2011). Improving bioavailability and stability of genistein by complexation with high-amylose corn starch. *Journal of Agricultural and Food Chemistry, 59*, 7932-7938.

Conde-Petit, B., Escher, F., & Nuessli, J. (2006). Structural features of starch-flavor complexation in food model systems. *Trends in Food Science & Technology, 17*(5), 227-235.

Godet, M. C., Buléon, A., Tran, V., & Colonna, P. (1993). Structural features of fatty acid-amylose complexes. *Carbohydrate Polymers, 21*(2), 91-95.

Guichard, E. (2002). Interactions between flavor compounds and food ingredients and their influence on flavor perception. *Food Reviews International, 18*(1), 49-70.

Higuchi, T. (1961). Rate of Release of Medicaments from Ointment Bases Containing Drugs in Suspension. *Journal of Pharmaceutical Sciences, 50*(10), 874-875.

Kohyama, K., & Nishinari, K. (1991). Effect of soluble sugars on gelatinization and retrogradation of sweet potato starch. *Journal of Agricultural and Food Chemistry, 39*, 1406-1410.

Kong, L., & Ziegler, G. R. (2014a). Formation of starch-guest inclusion complexes in electrospun starch fibers. *Food Hydrocolloids, 38*, 211-219.

Kong, L., & Ziegler, G. R. (2014b). Molecular encapsulation of ascorbyl palmitate in preformed V-type starch and amylose. *Carbohydrate Polymers, 111*, 256-263.

Lalush, I., Bar, H., Zakaria, I., Eichler, S., & Shimoni, E. (2005). Utilization of amylose-lipid complexes as molecular nanocapsules for conjugated linoleic acid. *Biomacromolecules, 6*(1), 121-130.

Lay Ma, U. V., Floros, J. D., & Ziegler, G. R. (2011). Formation of inclusion complexes of starch with fatty acid esters of bioactive compounds. *Carbohydrate Polymers, 83*(4),

1869-1878.
Lesmes, U., Cohen, S. H., Shener, Y., & Shimoni, E. (2009). Effects of long chain fatty acid unsaturation on the structure and controlled release properties of amylose complexes. *Food Hydrocolloids, 23*, 667-675.
Madene, A., Jacquot, M., Scher, J., & Desobry, S. (2006). Flavour encapsulation and controlled release – a review. *International Journal of Food Science & Technology, 41*(1), 1-21.
Nishiyama, Y., Mazeau, K., Morin, M., Cardoso, M. B., Chanzy, H., & Putaux, J.-L. (2010). Molecular and crystal structure of 7-fold V-amylose complexed with 2-propanol. *Macromolecules, 43*, 8628-8636.
Nuessli, J., Putaux, J. L., Bail, P. L., & Buléon, A. (2003). Crystal structure of amylose complexes with small ligands. *International Journal of Biological Macromolecules, 33*, 227-234.
Obiro, W. C., Sinha Ray, S., & Emmambux, M. N. (2012). V-amylose structural characteristics, methods of preparation, significance, and potential applications. *Food Reviews International, 28*, 412-438.
Oguchi, T., Yamasato, H., Limmatvapirat, S., Yonemochi, E., & Yamamoto, K. (1998). Structural change and complexation of strictly linear amylose induced by sealed-heating with salicylic acid. *Journal of the Chemical Society, Faraday Transactions, 94*, 923-927.
Osman‐Ismail, F., & Solms, J. (2010). Interaction of potato starch with different ligands. *Starch - Stärke, 24*(7), 213-216.
Rondeau-Mouro, C., Le Bail, P., & Buléon, A. (2004). Structural investigation of amylose complexes with small ligands: inter-or intra-helical associations? *International journal of biological macromolecules, 34*(5), 251-257.
Rundle, R. E. (1947). The configuration of starch in the starch-iodine complex. V. Fourier projections from X-ray diagrams. *Journal of the American Chemical Society, 69*, 1769-1772.
Siepmann, J., & Peppas, N. A. (2011). Higuchi equation: derivation, applications, use and misuse. *International Journal of Pharmaceutics, 418*(1), 6-12.
Tan, L., & Kong, L. (2019). Starch-guest inclusion complexes: Formation, structure, and enzymatic digestion. *Critical Reviews in Food Science and Nutrition*, 1-11.
Tapanapunnitikul, O., Chaiseri, S., Peterson, D. G., & Thompson, D. B. (2007). Water solubility of flavor compounds influences formation of flavor inclusion complexes from dispersed high-amylose maize starch. *Journal of agricultural and food chemistry, 56*(1), 220-226.
Uchino, T., Tozuka, Y., Oguchi, T., & Yamamoto, K. (2002). Inclusion compound formation of amylose by sealed-heating with salicylic acid analogues. *Journal of Inclusion Phenomena and Macrocyclic Chemistry, 43*, 31-36.
Yamashita, Y., Ryugo, J., & Monobe, K. (1973). An electron microscopie study on crystals of amylose V complexes. *Microscopy, 22*(1), 19-26.

Zaslow, B. (1963). Characterization of a second helical amylose modification. *Biopolymers, 1*, 165-169.

Zobel, H. F., French, A. D., & Hinkle, M. E. (1967). X-Ray diffraction of oriented amylose fibers. II. Structure of V amyloses. *Biopolymers, 5*, 837-845.